Attachment of VLDL Receptors to an Icosahedral Virus along the 5-fold Symmetry Axis: Multiple Binding Modes Evidenced by Fluorescence Correlation Spectroscopy†

Juergen Wruss,‡ Dominik Rünzler,§ Christina Steiger,‡,|| Peter Chiba,⊥ Gottfried Köhler,§ and Dieter Blaas*,‡

Max F. Perutz Laboratories, University Departments at the Vienna Biocenter, Department of Medical Biochemistry, Medical University of Vienna, Dr. Bohr Gasse 9/3, A-1030 Vienna, Austria, Max F. Perutz Laboratories, Department of Chemistry, University of Vienna, Campus Vienna Biocenter 5/1, 1030 Vienna, Austria, and Center for Physiology and Pathophysiology, Institute for Medical Chemistry, Medical University of Vienna, Währingerstrasse 13, 1090 Vienna, Austria

Received February 7, 2007; Revised Manuscript Received March 20, 2007

ABSTRACT: Human rhinoviruses (HRVs) are composed of 60 identical subunits, each comprising one copy of the viral capsid proteins VP1, 2, 3, and 4. Consequently, 60 symmetry-related epitopes are available for binding of antibodies or receptors. The minor receptor group of HRVs uses members of the low-density lipoprotein receptor family for cell entry. The ligand binding domains of these receptors are composed of various numbers of ligand binding repeats, and several of these modules within a single molecule are believed to attach simultaneously to the star-shaped dome at the 5-fold symmetry axis of the virus. Using fluorescence correlation spectroscopy (FCS), we have now determined the equilibrium binding constants and the mode of attachment of recombinant concatemers of ligand binding module 3 of the human very-low-density lipoprotein receptor to HRV2. We demonstrate that the avidity of the interaction drastically increases with the number of concatenated modules. For the trimer, the binding isotherm was biphasic, indicating that attachment of two and of three modules within the same molecule was resolved. The receptor consisting of seven repeats was found to bind most strongly, but a complete binding isotherm could not be established due to cross-linking of virions. The values of the dissociation constants were about 1 order of magnitude higher than those previously determined by using surface plasmon resonance techniques reflecting the different presentation of the binding partners. As compared to the concatemers, the natural receptors are composed of similar but not identical repeats; thus, cooperativity and different specificity of the ligand-binding modules allow for recognition of many ligands and viral serotypes. Due to the low concentrations and amounts of sample required, FCS is ideally suited for the determination of receptor binding parameters of viruses difficult to produce in high quantities and/or concentrations.

About half of all mild infections of the upper respiratory tract are caused by the 99 so far described serotypes of human rhinovirus (HRV). These viruses exhibit $T = 1$, pseudo $T = 3$ icosahedral symmetry and are roughly 30 nm in diameter. Like all other members of the family *Picornaviridae*, they contain a positive sense, single strand RNA genome that is translated into a polyprotein of about 300 kDa as soon as it arrives in the cytosol of the host cell. This protein is cotranslationally and autocatalytically cleaved into the capsid proteins VP1, VP2, VP3, and VP4, and seven (not including their precursors) nonstructural polypeptides providing the various enzymatic activities required for viral replication (*1*). In addition to the phylogenetic division into the subgenera HRV-A and HRV-B (*2*), rhinoviruses have also been classified according to their receptor specificity (*3*). Major group HRVs (87 serotypes) bind intercellular adhesion molecule 1 (ICAM-1) (*4*), and minor group HRVs (12 serotypes) (*5*) use members of the low-density lipoprotein receptor (LDLR) family for cell attachment (*6*).

ICAM-1 exhibits a typical immunoglobulin fold, and its five domains are arranged almost linearly, resulting in a rodlike appearance in electron microscopy images (*7*). As seen from cryo-electron microscopy (cryo-EM) image reconstruction, 60 copies of a soluble fragment of ICAM-1 attach, via their N-terminal domain, to major group HRVs (such as HRV3, 14, and 16) within a cleft or canyon encircling the star-shaped dome at each of the 12 5-fold axes of icosahedral symmetry (*8*−*10*). Therefore, a major group virus can bind 60 individual soluble receptor molecules.

LDL receptors are unrelated to ICAM-1. Their ligand binding domains are composed of 7 (LDLR), 8 (very-LDLR; VLDLR), and 31 (LDLR related protein; LRP) modules with very similar sequences and three-dimensional structures;

† This work was supported by the Austrian Science Foundation Grant #P17516-B10 and the Austrian Nanoinitiative N209.

* Corresponding author. Phone: ++43-1-4277-61630. Fax: ++43-1-4277-9616. E-mail: dieter.blaas@meduniwien.ac.at.

‡ Max F. Perutz Laboratories, University Departments at the Vienna Biocenter, Department of Medical Biochemistry, Medical University of Vienna.

§ Max F. Perutz Laboratories, Department of Chemistry, University of Vienna.

|| Current address: Division of Immunology, Infection and Inflammation, Glasgow University Research Centre, Glasgow, G128TA, U.K.

⊥ Center for Physiology and Pathophysiology, Institute for Medical Chemistry, Medical University of Vienna.

10.1021/bi700262w CCC: $37.00 © 2007 American Chemical Society
Published on Web 05/02/2007

there are a number of other members of this family that most probably do not have any function in virus attachment (*11*). The modules composing the ligand-binding domain are about 40 residues long and are stabilized by a central Ca ion and three disulfide bridges. Cryo-EM reconstruction showed that these receptors do not bind within the canyon but rather attach to the BC, DE, and HI surface loops of VP1 that form a dome or plateau at the 5-fold axis. The X-ray structure of a complex between the minor group virus HRV2 and a soluble VLDLR fragment encompassing modules 2 and 3 (V23) revealed that the footprint of the individual repeats extends over two symmetry related subunits. Due to a resolution of only 3.5 Å and to the similarity of the amino acid sequences of modules 2 and 3, it was not possible to discriminate between attachment of V3 only (with V2 being disordered) and simultaneous attachment of V2 and V3 to two symmetry related sites. The latter arrangement is consistent with the observed 80% occupancy resulting from two molecules of V23 attached to each 5-fold axis leaving the fifth site unoccupied (i.e., a stoichiometry of 1:24) (*12*). It is also supported by the strong increase in affinity and virus-neutralization capacity correlated with the number of repeats present in the receptor fragment (ref *13* and this report).

The interpretation of avidity effects resulting from the multimodular structure of the receptors is difficult within the context of the natural proteins because their modules are similar but not identical. Thus, their affinity for a given binding site might differ. Furthermore, some of the modules lack the tryptophan residue and/or the acidic center chelating the Ca ion that play a key role in the interaction with the virus and might not function in binding. For that reason we used artificial concatemers of repeat three of human VLDLR in the binding experiments. The recombinant proteins were expressed with maltose binding protein (MBP) fused to their N-termini and a hexa-his tag fused to their C-termini. The former strongly enhances folding and solubilization whereas the latter facilitates purification (*14*).

Capillary electrophoretic analysis of a complex of HRV2 saturated with such a receptor construct consisting of 5 copies of module 3 arranged in tandem (MBP-V33333) suggested a stoichiometry of 1:12, i.e., 12 receptor molecules would attach per virion (*15*). This again indicates that all five modules might be simultaneously implicated in binding. Recently, the X-ray structure of a complex between HRV2 and V33333 was solved; unexpectedly it showed only 60% occupancy suggesting that, on average, not all five but rather only three modules per receptor molecule may be involved (*16*). In order to analyze the contribution of single modules to the overall binding strength, the equilibrium binding constants of the interaction between various soluble V3 concatemers and HRV2 had been determined by surface plasmon resonance (SPR) methodology. These experiments showed a substantial increase in functional affinity with the number of repeats, again pointing to the involvement of several modules in binding (*13*). However, the unexpectedly high affinities obtained, e.g., with a $K_D < 10^{-12}$ mol/L for the V3 pentamer, pointed to the well-known problematic of SPR measurements with respect to surface (re)binding effects. This prompted us to complement this previous study (*13*) by applying fluorescence correlation spectroscopy (FCS) (*17*) as a true solution-based technique to avoid these adverse effects. FCS requires only minute amounts of components, typically less than 10 μL in the nanomolar concentration range. It also allows for completion of a whole set of measurements sufficient to obtain an entire binding isotherm within minutes. Employing Cy3 fluorescence labeling we determined the affinities of the receptor−virus interactions of the entire set of V3 concatemers.

MATERIALS AND METHODS

Virus. HRV2, as originally obtained from the American Type Culture Collection (ATCC), was grown in HeLa-H1 cells in suspension culture and purified as described (*12*).

Construction, Expression, and Purification of V3 Concatemers. Soluble receptor fragments were prepared essentially as described previously (*12*, *13*, *15*). Briefly, DNA encoding human V3 was amplified with *Pfu* DNA-polymerase from a vector encoding the entire ligand-binding domain of human VLDLR (*6*) using primers 5′-ATGCGGATCCAACATGCCGCATACATG and 5′-GCAGCCCGGGACTCATATGGCACTGTTC, and the fragment was introduced into the vector pMalc2b (New England Biolabs), using restriction sites for *Bam*HI and *Xma*I. The resulting plasmid encodes V3 (amino acid residues 112 to 151 of the VLDLR sequence) fused at the N-terminus to MBP via an 11 amino acid linker. Due to the cloning procedures, the protein had an extension of 20 amino acid residues (including a his_6-tag) at its C-terminus. To produce V3 concatemers, this DNA was cleaved with *Sma*I to generate blunt ends 3′ of the V3 sequence. Another fragment encoding V3 was synthesized via PCR using primers 5′-GGGACATGCCGCATACATGAAATC and 5′-ATTGCCACAGTTTTCTTCATC. This fragment was ligated into the *Sma*I site resulting in a V33 dimer with an additional proline between the two modules. After transformation, colonies containing plasmids with 1, 2, 3, or 4 copies of V3 were obtained. To generate longer concatemers, the plasmid encoding MBP-V3333 was digested with *Sma*I and ligated with the same PCR fragment as above. This gave rise to additional concatemers with 5 and 7 V3 repeats fused to MBP. Expression, purification, and refolding of the soluble receptors were then carried out as described previously (*14*) with the following modifications. *Escherichia coli* TB1 was transformed with the respective plasmids, grown to $0.7A_{600}$, and induced with 0.3 mM IPTG at 28 °C for 20 h. Bacteria from a 1 L culture were pelleted, resuspended in 45 mL of Tris-buffered saline plus 2 mM $CaCl_2$ (TBSC), and sonicated. Insoluble fragments were pelleted for 10 min at 4.3 krpm in a Kendro Megafuge 1.0R followed by centrifugation for 20 min at 14 krpm in an SS34 fixed angle rotor in a Sorvall centrifuge. The supernatant was incubated overnight with 5 mL of a 50% slurry of Ni-NTA beads (Sigma) in a rolling tube. Beads were pelleted for 5 min at 2.2 krpm and washed twice with 50 mL of TBSC containing 20 mM imidazole. Bound protein was eluted with 20 mL of TBSC containing 150 mM imidazole, dialyzed against TBSC, and refolded using a 10 mM cystamine/100 mM cysteamine redox system. Proper folding, as indicated by binding activity, was verified in a virus overlay blot by using [^{35}S]-labeled HRV2 (*18*).

Labeling of HRV2 with FITC. Purified HRV2 was dialyzed against 100 mM sodium bicarbonate adjusted to pH 9.0 with NaOH and mixed with FITC in DMSO at 500-fold molar

excess. After 2 h in the dark, excess FITC was removed by size exclusion chromatography using a Sephadex G100 column. Purity of the virus and absence of free dye were checked by capillary electrophoresis (*19*).

Labeling of Receptor Fragments with Cy3. Since V3 lacks lysine residues and no lysines were introduced by the cloning procedure, the only free amino group appears after cleavage with factor Xa between MBP and the first V3 module (*14*). The resulting concatemers, now without MBP, were repurified over a Ni-NTA column and dialyzed against TBSC. For labeling the proteins with Cy3 (Amersham Biosciences, Piscataway, NJ) at the N-terminus, they were first dialyzed against 150 mM NaCl containing 2 mM $CaCl_2$, followed by dialysis against 100 mM $NaHCO_3$, 2 mM $CaCl_2$. Fluorescence labeling was carried out for 1 h according to the supplier's instructions. To remove excess free dye, the samples were dialyzed against TBSC. Finally, the labeled proteins were purified over a Superdex 75 (Pharmacia) column using an Äkta purifier (GE Healthcare). The number of dye molecules incorporated per protein molecule was determined spectrophotometrically using the formula dye/protein $= \{1.13 \times A_{552}\}/\{A_{280} - (0.08 \times A_{552})\}$. Protein concentrations were determined from the absorption at 280 nm (with molar extinction coefficients calculated from the amino acid composition) and by the Bradford assay with essentially the same result.

Fluorescence Correlation Spectroscopy Setup. FCS measurements were carried out on a Confocor spectrofluorimeter (Carl Zeiss, Germany) equipped with a water immersion objective (C-Apochromat 63×/1.2 W Korr), an avalanche photodiode (SPCM-CD 3017), and a hardware autocorrelator (ALV 5000, AVL, Langen, Germany). FITC-labeled HRV2 samples were excited with an Ar-laser (Lasos, Germany) attenuated by optical density filters. The 488 nm line was selected by using an excitation filter (450−490 nm). The pinhole diameter was adjusted to 45 μm, resulting in a diameter of the confocal volume element of 0.34 μm in the radial and 2.4 μm in the axial dimension as determined by calibration measurements with rhodamine-6G. To assess the accuracy of the size measurements in the high diameter range, fluorescent polystyrene beads of 20 nm diameter (Invitrogen) were used. Fluorescence emission of FITC-labeled HRV2 was detected through a dichroic mirror (510 nm) followed by a long-pass filter (515 nm). Cy-3 labeled receptor fragments were excited at 543.5 nm with a HeNe laser (Uniphase, Manteca, CA) attenuated by optical density filters. The pinhole diameter was also adjusted to 45 μm, resulting in a diameter of the confocal volume element of 0.38 μm in the radial and 2.3 μm in the axial dimension as determined by calibration with rhodamine-B. Fluorescence emission was detected through a dichroic mirror (580 nm) with a long-pass filter (590 nm). Measurements were made using 24-well borosilicated cover glass AssayChips (Evotec Technologies, Germany) with a maximal volume of 25 μL per well. The focus was adjusted 150 μm above the upper side of the slide. Loss of Cy-3 labeled receptor proteins due to adsorption to the glass surface could be prevented by coating with human serum albumin (2 mg/mL in water for 17 min at 4 °C, followed by three washings with water and air-drying). Coated AssayChips were stored at 4 °C and used within 36 h.

Fluorescence autocorrelation functions of Cy3-labeled receptor concatemers were obtained in the absence and in the presence of HRV2 at various concentrations by 10 to 20 independent measurements with a data acquisition time of 10 s each. All FCS measurements of virus−receptor association were carried out using 5 μL of Cy3-labeled receptor at a constant concentration of 1×10^{-7} mol/L in TBSC mixed with 5 μL of a geometric concentration series of HRV2 in TBSC as given in the figures. The mixtures were incubated for 5 min at room temperature or for 30 min at 4 °C prior to measurements. The translational diffusion times were calculated with the FCS ACCESS software (Version 1.0.12, Evotec Technologies, Germany).

Data Analysis. The normalized autocorrelation function $G(\tau)$ was used to describe time-dependent fluctuations around the mean fluorescence intensity F. Ensemble averages are denoted by angular brackets:

$$G(\tau) = 1 + \langle \delta F(t) \cdot \delta F(t+\tau) \rangle / \langle F \rangle^2 \qquad (1)$$

The analytical form of $G(\tau)$ depends on both the geometry of the Gaussian confocal volume and the diffusion properties of a single diffusing fluorescent species and is given by

$$G(\tau) = 1 + 1/[N(1 + \tau/\tau_D)(1 + \tau/(z/r)^2\tau_D)^{0.5}] \qquad (2)$$

where the fluorescent species is characterized by the particle number N and the diffusion time τ_D. The confocal volume with z as axial dimension and r as radial dimension is calculated by the relationship $D = r^2/4\tau_D$ based on calibration measurements using rhodamine-6G with the known diffusion coefficient $D = 2.8 \times 10^{-10}$ m^2 s^{-1}. Experimental autocorrelation functions were evaluated using a one-component model including the triplet state with the triplet fraction F_T and the triplet lifetime τ_T

$$G(\tau) = \frac{1}{N'}[g_D(\tau)][F_T e^{\tau/\tau_T} + (1 - F_T)] + 1 \qquad (3)$$

with $N' = N(1 - F_T)$ and

$$g_D(\tau) = \left(1 + \frac{\tau}{\tau_D}\right)^{-1}\left(1 + \frac{\tau}{(z/r)^2\tau_D^2}\right)^{-0.5} \qquad (4)$$

In addition, the data were evaluated using a two-component model as described previously (*20*). Importantly, in FCS there is no need to separate bound from free ligand but a change in the measured mean diffusion time can only be observed when the fraction of bound ligand is not negligible. Therefore, the assumption that the concentration of ligand free in solution equals the concentration of ligand added to the solution is no longer valid. Consequently, total binding as a function of added ligand and ligand depletion have to be taken into account in the nonlinear regression analysis of the binding isotherms. In the particular case considered here, the fluorescently labeled V3 concatemers are the "ligands" and the virus particles function as "receptors" possessing 60 independent binding sites.

A one-step or monophasic binding model is defined by the increase of the mean diffusion time τ_D from that of the free receptor τ_R to the diffusion time τ_{RV1} of the saturated receptor−virus complex:

$$\tau_D = \tau_R + (\tau_{RV1} - \tau_R)\frac{\alpha - \sqrt{\alpha^2 - 4c_V c_R}}{2c_R} \quad (5)$$

with $\alpha = c_V + c_R + K_{D1}$, where c_V is the respective virus concentration, c_R is the total concentration of receptor, and K_{D1} is the equilibrium dissociation constant of the receptor−virus complex in the monophasic binding model. The diffusion time of the free receptor, as determined in the absence of virus, was treated as an additional constant.

The biphasic binding model assumes the simultaneous presence of two types of receptor−virus complexes; in the first one the receptor molecules are bound via all modules whereas in the second one not all ligand binding domains take part in attachment. This model was defined accordingly with the diffusion time τ_{RV2} for this second type of receptor−virus complex and the corresponding K_{D2} as additional variables:

$$\tau_D = \tau_R + (\tau_{RV1} - \tau_R)\frac{\alpha - \sqrt{\alpha^2 - 4c_V c_R}}{2c_R} + (\tau_{RV2} - \tau_{RV1})\frac{\beta - \sqrt{\beta^2 - 4c_V c_R}}{2c_R} \quad (6)$$

with $\alpha = c_V + c_R + K_{D1}$ and $\beta = c_V + c_R + K_{D2}$. The resulting binding isotherms were evaluated by both binding models applying a Marquardt nonlinear least-squares algorithm (Origin, Microcal). The calculated profiles of the residuals and the corresponding correlation coefficients were used to compare the quality of the monophasic with that of the biphasic fits.

RESULTS

Fluorescence correlation spectroscopy derives the diffusion time τ of fluorophore-labeled molecules in solution from the autocorrelation of fluorescence fluctuations within a small detection volume (in our setup about 0.2 fL). These fluctuations, caused by the molecules moving through the volume, are recorded with a confocal microscope equipped with an avalanche photodiode with single photon sensitivity. Based on calibration of the observation volume with a small M_r dye of known diffusion coefficient, the diffusion coefficient D of the analyte is determined and the radius r of the molecule is calculated using the Stokes−Einstein equation $r = kT/6\pi\eta D$ with the Boltzmann constant $k = 1.3807 \times 10^{-23}$ kg m^2 s^{-2} K^{-1}, the viscosity of the solution $\eta_{298K} = 0.89 \times 10^{-3}$ kg m^{-1} s^{-1}, and the temperature $T = 298$ K.

Determination of the Apparent Diameters of Virus and Receptor. We first attempted to determine the diffusion constants of the Cy3-labeled MBP-receptor fusion proteins. However, as seen from the inhomogeneous fluorescence fluctuations, the material appeared to contain aggregates that could not be removed by centrifugation or filtration (data not shown). This aggregation is presumably due to the hydrophobic nature of the dye. We did not determine the number of Cy3 molecules attached per fusion protein, but owing to the presence of 36 lysine residues in the MBP moiety many dye molecules can be incorporated; this might strongly increase the overall hydrophobicity of these recombinant receptors and render them very sticky. Therefore, for all further experiments, we removed the MBP via cleavage with factor Xa followed by affinity chromatography (*14*) prior to labeling.

The V3 ligand binding repeats and the linkers lack lysine residues. Consequently, no more than a single dye molecule becomes incorporated at the N-terminus of various concatemers that now showed typical FCS autocorrelation curves. Because there are 8 additional amino acid residues at the N-terminus and 20 (including the his_6-tag) at the C-terminus that are not present in the natural V3 repeat, the V3 construct exhibits a M_r of 12 kDa and each additional module accounts for roughly 9 kDa (*13*). The repeats are ellipsoid with half axes of about 1 and 1.4 nm (in the direction of the N to the C terminus) (*12*, *21*). Furthermore, as deduced from NMR data, individual modules within the molecule can move freely with respect to each other (*22*). Therefore, the overall size of the concatemers can only be estimated from the average of all possible conformations the molecules adopt in solution. For V33333 ($M_r = 52$ kDa), the upper limit of the radius r for the extended conformation of the molecule is thus roughly 7 nm. From the diffusion constant of V33333 (3.1×10^{-11} m^2 s^{-1}) a radius of 8 nm was calculated, which is close to the 7 nm as estimated above. The diffusion time increased with the number of modules constituting the respective molecule from 150 μs (V3) to 400 μs (V3333333; Figure 2). The concentrations derived from the autocorrelation functions corresponded within 60−80% rather well to the spectrophotometrically determined protein concentrations.

We also determined the diffusion coefficient of HRV2 alone, employing FITC-labeled virions (*23*). The measured diffusion time of 760 ± 80 μs yielded a diffusion constant of 9.5×10^{-12} m^2 s^{-1} corresponding to a hydrodynamic diameter of the virus of about $d = 51 \pm 5$ nm. This value is roughly by 70% bigger than the ∼30 nm as derived by electron microscopy (*24*) and X-ray crystallography (*25*). The size of the diffusing particles is little less than 1/10 of the diameter of the confocal volume (340 nm in the radial dimension) and thus not negligible. This became apparent when measuring polystyrene particles with a nominal diameter of 20 nm. Their diffusion times translated into an apparent diameter of 28 nm (not shown). These results indicate an overestimation of 40% for particles in this size range. When this factor is taken into account, the apparent diameter of the virus corrects to 33 nm, which is close to the 30 nm determined by the other methods.

Determination of the Equilibrium Binding Isotherms. In FCS, the binding parameters are deduced from the increase in the mean diffusion coefficient of a comparably small fluorescent molecule upon attachment to a much bigger binding partner. When a Cy3-labeled V3 receptor module attaches to the virus, its apparent diffusion constant is expected to decrease by 1 order of magnitude from between 6.0×10^{-11} (V3) and 3.0×10^{-11} (V33333) to less than 9.5×10^{-12} m^2 s^{-1}. These calculated diffusion constants correspond to expected diffusion times of between 150 μs and 760 μs, values easily accessible to FCS measurement.

First, samples of Cy3-labeled receptors at a constant concentration of 1×10^{-7} mol/L were mixed with virus at 3.7×10^{-6} mol/L. After incubation for 5 min at room temperature, the count rates and derived fluorescence autocorrelation curves were determined and compared with that of receptor alone. Except from V3333333 (Figure 1; right

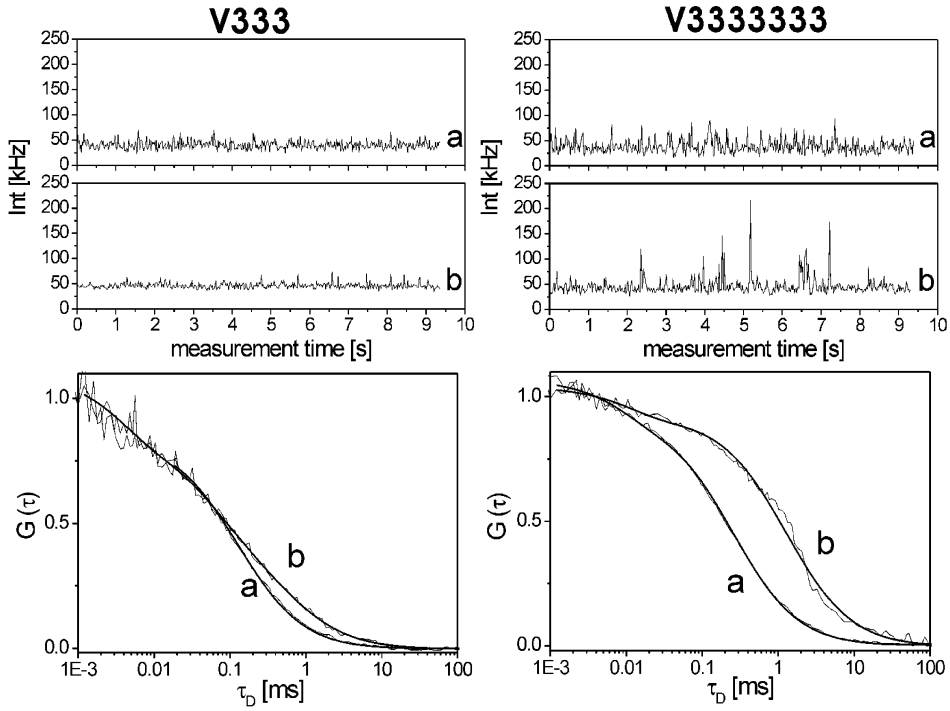

FIGURE 1: Fluorescence correlation measurements of the binding of Cy3-labeled receptors to HRV2. For V333 (left) and V3333333 (right), the intensity fluctuations (upper panels) and corresponding normalized autocorrelation curves (lower panels) of free receptor at 50 nmol/L (a) and receptor (50 nmol/L) plus virus at 3.7 μmol/L (b) are depicted. The curves of free V3, V33, V3333, and V33333 (not shown) were very similar to that of free V333. Note that the profiles of V333 alone and complexed to virus show an even distribution of the fluctuations whereas the V3333333 complex shows spikes of fluorescence intensity up to five times higher than the average indicating the presence of aggregates.

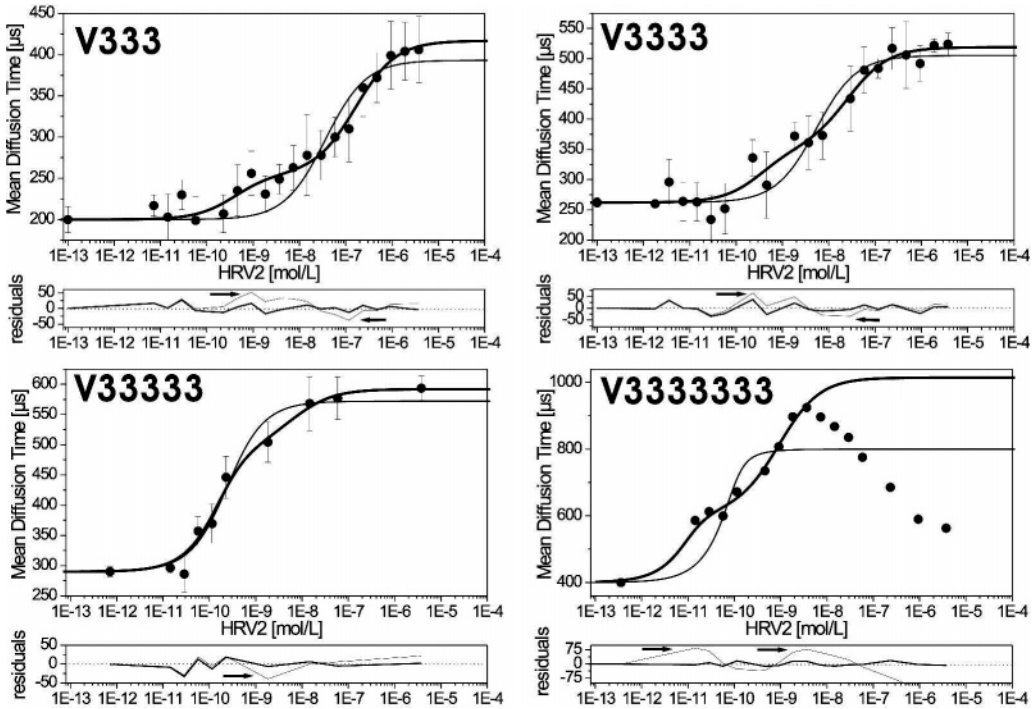

FIGURE 2: Binding isotherms of the attachment of V3 concatemers to HRV2. The respective Cy3-labeled soluble receptor derivatives were mixed with a geometrical dilution series of HRV2 to result in a final concentration of the receptors of 50 nmol/L and of the virus as depicted. After incubation at room temperature for 5 min, the fluorescence correlations were measured and the mean diffusion times were determined. Thin lines represent a monophasic fit, the thick lines a biphasic fit. Bottom panels depict the residuals. Arrows indicate residuals not equally distributed around zero. Bars denote mean and standard deviation from 30 measurements. Note that in the case of V3333333 the data of several measurements were discarded because of the presence of too many spikes and thus no standard deviation is shown. For correlation coefficients see Table 1.

panels), all concatemers gave rise to intensity fluctuation profiles and autocorrelation curves of the expected shape (exemplified for V333 in Figure 1, left panels). In the intensity fluctuation profile of the mixture between HRV2 and V3333333 (Figure 1, right panel b), a number of spikes occurred probably because of the presence of cross-linked

Table 1: Goodness of Fit of the Experimental Binding Data to a Monophasic and a Biphasic Model as Shown in Figure 2

	R^2 for type of model	
concatemer	monophasic	biphasic
V333	0.90	0.98
V3333	0.95	0.97
V33333	0.97	0.98

viruses. As expected, upon addition of virus, a clear shift of the autocorrelation curves toward longer diffusion times was observed. However, the diffusion time corresponding to free virus was never attained since the measurement determines the mean of all moving fluorescent species; this indicates that a considerable fraction of receptor molecules had not attached to virus and free receptors were still present in the mixture. A similar behavior was seen for V3, V33, V3333, and V33333 although the shift in the presence of virus was barely visible for V3 and V33, indicating that only a very small fraction of the receptors was present as complexes even at the highest possible virus concentration (not shown).

The next set of experiments was carried out again with a constant concentration of the receptors but with a serial geometric dilution of virus. According to Meseth and colleagues (*26*) the diffusion times must differ at least by a factor of 1.6 to distinguish between two different molecular species in solution under the assumption of comparable quantum yields. Such a difference was only observed at the highest virus concentration used (Figure 2). Therefore, application of a two-component model would give better results only for this part of the binding isotherm. However, as the major part of it is better described by a one-component model, we used this latter model to fit the entire binding isotherms.

In order to derive the equilibrium binding constants, the virus concentration was plotted against the diffusion time and the points were fitted to a monophasic equilibrium binding isotherm (Figure 2). Interestingly, the fits were poor (thin lines) and showed big deviations in two regions (see thin line of the residuals plot below each panel). The attempt at better fitting the points with a biphasic equation was more successful and a clear difference in the goodness of the fit was obvious for V333 (Figure 2, thick lines and correlation coefficients in Table 1). Although many spikes were present in the intensity fluctuation profile of the binding reaction between HRV2 and V3333333 (see Figure 1, right panels), a concentration-dependent increase of the diffusion time was seen up to roughly 20 nmol/L of HRV2. Beyond this value the diffusion time decreased again. This is presumably because of aggregation and precipitation of receptor−virus complexes reducing their concentration in the confocal volume. When fitting the points only up to this concentration, a fairly reasonable biphasic fit was obtained (last panel in Figure 2) that looked quite similar to that of the other receptors. Nevertheless, due to this inhomogeneity of the count rate, caused by the presence of cross-linked virions, for V3333333, quantitative data should be interpreted with caution.

Complete equilibrium binding isotherms can be obtained only if the concentrations of both binding partners are higher than the K_D of the interaction. Apparently, this was the case for V333, V3333, and V33333. The mean diffusion time of these soluble receptors typically doubled at the highest concentration of HRV2 and leveled into a plateau. Nevertheless, the highest value measured was still below the diffusion time of free virus. As already mentioned above, this indicates the presence of a substantial fraction of free receptor. The affinities of the monomer V3 and the dimer V33 were too low even at the highest virus concentration technically achievable, and no such plateau was evident. Therefore, only the initial part of the isotherm was accessible. To obtain at least an approximation for the affinity values of these weakly binding receptors, the curves were extrapolated accordingly.

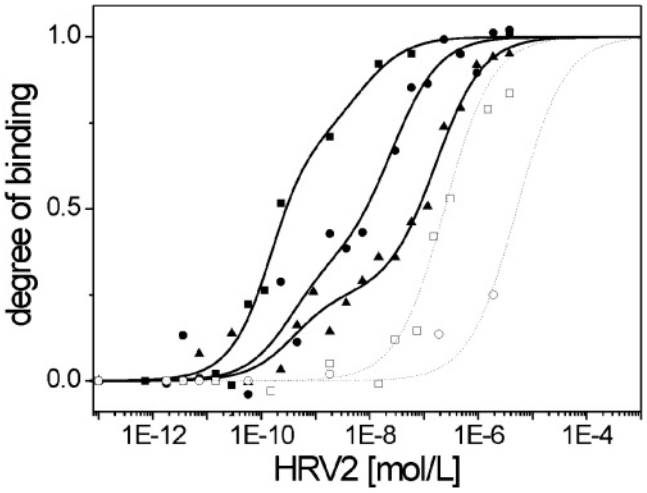

FIGURE 3: Degree of binding of receptor concatemers as a function of virus concentration. Monophasic fits are shown for V3 (○) and V33 (□), and biphasic fits are shown for V333 (▲), V3333 (●), and V33333 (■). Since no full equilibrium binding isotherms could be derived from the data of V3 and V33, the curves were extrapolated accordingly as to reach the same plateau at the highest virus concentrations (dotted lines).

The equilibrium binding isotherms for all receptors (this time normalized, i.e., to the degree of binding) are depicted in Figure 3. The derived dissociation constants are summarized in Table 2 and compared to values obtained from SPR measurements (*13*).

DISCUSSION

In our experimental setup, the receptor was present at a constant initial concentration of 50 nmol/L with the virus added to final concentrations of between 2 pM and 5 μmol/L (see Figure 2 and 3). Fifty nanomoles of V33333 saturate 4.2 nmol of virus (i.e., 50 nmol of binding sites) whereas 12 molecules of V333 can attach via three modules and another 12 via two modules (i.e., 8.4 nmol of virus). Thus, saturation cannot occur beyond these virus concentrations. Furthermore, even when taking the high affinity dissociation constants in Table 2, a simple calculation shows that saturated V333 complexes cannot be formed in appreciable quantity under any of the conditions. In contrast to the SPR measurements (*13*), our FCS experiments were thus carried out under nonsaturation conditions (see Figure 5).

Biphasic binding, as observed in the particular case of the present experiments, is due to different affinities of individual receptor molecules attaching via different numbers of modules. As shown by the modeled binding isotherms in Figure 4, biphasic behavior can only be observed as long as the receptor concentration is of the same order of magnitude

Table 2: Comparison of Dissociation Constants (K_D [mol/L]) Derived from FCS and SPR Data

	FCS			SPR	
	monophasic	biphasic			
receptor	K_D	K_{D1}	K_{D2}	K_D	ratio FCS/SPR
V3	5.0×10^{-6}			4.5×10^{-7}	11
V33	2.4×10^{-7}			1.4×10^{-8}	17
V333	3.0×10^{-8}	6.5×10^{-9}	4.0×10^{-7}	3.7×10^{-10}	17
V3333	5.3×10^{-9}	2.9×10^{-10}	2.6×10^{-8}	1.6×10^{-11}	18
V33333	1.9×10^{-10}	9.6×10^{-11}	6.8×10^{-9}	$< 1 \times 10^{-12}$	nd[a]
V3333333	9.4×10^{-12}	$< 3 \times 10^{-12}$	5.0×10^{-10}	3×10^{-11}	nd

[a] Not determined.

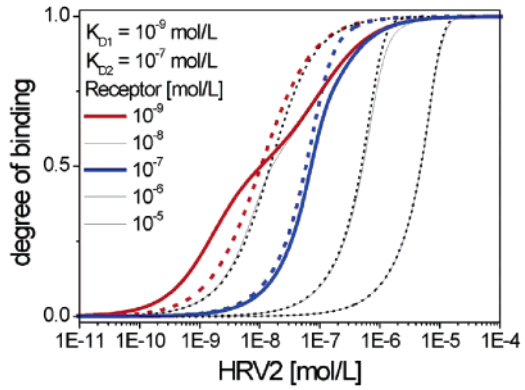

FIGURE 4: Model of the behavior of virus−receptor binding. The binding curves for the assumed K_Ds differ by 2 orders of magnitude (i.e., 10^{-9} and 10^{-7} mol/L, comparable to the values of V333) and are displayed for different concentrations of the receptor (i.e., from left to right 10^{-9} to 10^{-5} mol/L). Full lines show models of the biphasic binding and dotted lines of the monophasic binding. The blue line corresponds to a receptor concentration equal to the low affinity K_D (i.e., 10^{-7} mol/L); the red line corresponds to a receptor concentration equal to the high affinity K_D (i.e., 10^{-9} mol/L).

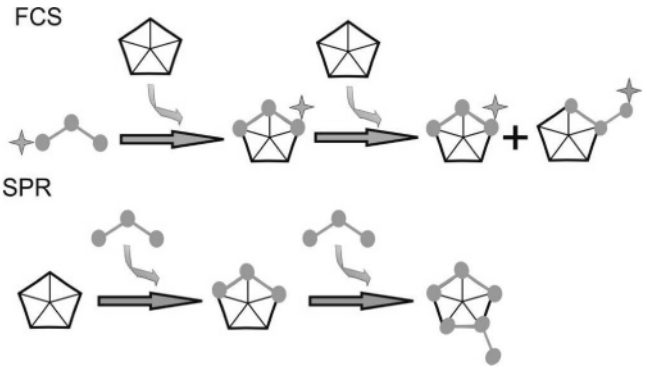

FIGURE 5: Schematic comparison of the binding modes observed in FCS and in SPR. In FCS, the receptor is present at limiting concentrations. As exemplified for V333, at equilibrium, this results in a mixed population of virus (depicted as pentamers) with its binding sites either unoccupied or carrying receptors attached via three or via two modules. In SPR, the virus is present at limiting concentrations, leading to its saturation with receptor molecules. In the case of V333 two molecules can bind to the same vertex via three and via two binding repeats. This results in complete coverage of the binding sites on the viral surface. Whether this effect occurs simultaneously or consecutively (as insinuated in the drawing) is not known. The starlike symbol represents the Cy3-label.

as the equilibrium binding constant of the reaction with the highest affinity. When taking $K_{D1} = 10^{-9}$ mol/L and $K_{D2} = 10^{-7}$ mol/L, values comparable to those obtained for V333 (6.5×10^{-9} mol/L and 4×10^{-7} mol/L, respectively), this is the case when the receptor concentration is $\sim 10^{-9}$ mol/L (full and dotted red lines for the biphasic and monophasic model, respectively, in Figure 4). With increasing receptor concentrations the difference between the respective binding isotherms vanishes (black lines). Already, at a receptor concentration equal to the low affinity K_{D2} (i.e., 10^{-7} mol/L) the biphasic and the monophasic traces are almost equal (compare blue lines). However, in these latter cases, the biphasic behavior is still recognizable via the asymmetry of the curves since the slope in the lower part is much flatter than the slope in the upper part. Importantly, the virus concentration range, where 10 to 90% of binding occurs, covers significantly more than 2 orders of magnitude (see also Figure 2 and 3 where this is most pronounced in the case of V333). However, as shown in this model, at exceedingly high receptor concentrations relative to both K_Ds this distinction is no longer possible. From the K_Ds summarized in Table 2, the biphasic behavior of V333 and V3333 is most evident. For V33333, the receptor concentration employed is higher than both K_Ds. Since the signal-to-noise ratio was too low at very low concentrations, as would be required to cover this range, a distinction between the two binding modes was impossible.

Taking into account only the first of the two dissociation constants, which corresponds to involvement of all modules making up the receptor molecule, it is significant that the K_Ds determined by FCS were about 20 times higher than those determined by SPR (Table 2). This is in accordance with previous findings, e.g., of Schubert and co-workers (*27*), who noticed a difference of the K_Ds by a factor of 20 to 25 when measuring DNA−protein interactions by SPR and FCS. They attribute the discrepancies to the different presentations of one of the binding partners, i.e., in one case immobilized (SPR) and in the other case free in solution (FCS). In addition, for the different setups the concentration of receptor varies within different ranges. Thus, in SPR, saturation can be easily attained whereas this is not the case in FCS as schematically depicted in Figure 5. Under saturating conditions, each pentamer would carry two copies of V333, one attached via three repeats and one via two repeats. Under nonsaturating conditions, as in FCS, some pentamers might carry receptors which are attached either via two or via three repeats. It was not possible to determine two components of the binding reaction in SPR, although the better fit of a "complex model" pointed already to two parallel binding reactions with different affinities. Furthermore, equilibrium binding constants for V33333 could not be derived by SPR because of technical limitations. FCS thus confirms and extends the findings of SPR in that both methods indicate biphasic behavior of the system. Keeping in mind that SPR

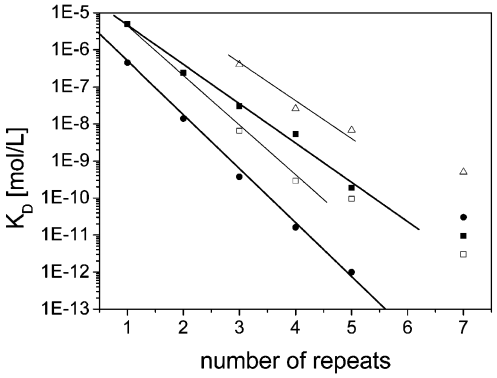

FIGURE 6: The free energy of binding increases by an equal amount for every additional module in the receptor. The K_D values from Table 2 were plotted versus the number of repeats in the concatemer as determined by FCS for monophasic (■) and biphasic (open symbols) fits. K_{D1} (□); K_{D2} (△). Previously derived SPR results (*13*) are also shown (●).

exaggerates the affinity due to surface effects, it nevertheless allowed for an estimation of the affinity of a single repeat, which was hardly possible in the FCS setup. Thus, taking into account the caveats mentioned above, the methods complement each other extending the measuring range at both the low and the high affinity range.

The standard Van't Hoff equation $\Delta G_B = -RT \log K_D$ relates the free energy of binding to the dissociation constant. In Figure 6 we plotted log K_D versus the number of repeats in the concatemer. The linear dependencies indicate that ΔG_B becomes more negative by an equal amount $\Delta\Delta G_B$, for every additional module in the receptor. The log K_D values for V3 and V33 and those of the high affinity component of the larger concatemers (log K_{D1}, see Table 2) lie on a line with an ascent of $\Delta\Delta G_B = -7 \pm 1$ kJ/mol per module. This value is in good agreement with SPR; the data points obtained with this method lie on an almost parallel line that is only shifted upward by a factor of 17 ± 2 (see also Table 2). Remarkably, from linear regression, a $K_D = 5 \pm 1$ μmol/L for the single receptor module was found that agrees very well with that estimated from the few measurable data points (see Figure 3). This value corresponds to a binding energy ΔG_B of -30 kJ/mol. As already pointed out, SPR yielded a roughly 20 times lower value of $K_D = 0.4 \pm 0.05$ μmol/L for a single module. Interestingly, although the two methods yield different absolute values, they give almost identical values for the increase in free binding energy per added module. However, the phenomenon of binding of single molecules via different numbers of repeats was not resolved by SPR. Most remarkably, for those concatemers whose low and high affinity binding components could be determined from the biphasic fit with confidence (V333, V3333, and V33333), the K_{D2} of V3*n* was very similar to the K_D (as derived from monophasic fit and thus combining the non-resolved K_{D1} and K_{D2}) of V3*n*−1 (see Table 2) indicating the validity of the measurements and of our model.

For V3333333 the K_D obtained from FCS measurement fits rather well the results for V3 to V33333, although only five modules can simultaneously bind to one binding site on the virus. The higher probability to find five consecutive modules for attachment to the virus should explain the lower dissociation constants obtained. Interestingly the discrepancy between an interpolated value for V3333333 and the measured ones is much larger for the SPR data than for FCS data.

$\Delta\Delta G_B$ for each additional binding module is considerably smaller than ΔG_B for the single repeat. Jenks has explained how such a change of the binding energy of covalently linked ligands can be viewed in terms of a connector Gibbs energy ΔG_S, which is largely, but not entirely, an entropy term (*28*). ΔG_B represents the change in the probability of binding as a consequence of the connection of the two subunits but also takes into account enthalpic terms like the strain energy related to conformational adaptation to the geometry of the multiple binding sites. Nevertheless, this rise in ΔG_B upon increasing the number of single repeats causes a decrease of 1 order of magnitude in the K_D for every module and thus a large increase of the binding affinity upon multimodular binding.

Multimodular receptor binding, as it occurs in minor group HRVs, allows for an enormous increase in binding strength combined with low recognition selectivity. In this way, 12 different viral serotypes are being recognized in the absence of any obvious sequence similarity of the binding site, except from the presence of a single conserved lysine residue. Utilizing this principle, LDL receptors, and in particular LRP, recognize a plethora of different ligands (*29*). This attachment mode contrasts with that of most other picornaviruses that bind their cognate receptors (ICAM-1 (*4*), the poliovirus receptor (*30*), integrins (*31*), and the coxsackie-adenovirus receptor (*32*)) via only one interaction site per receptor molecule. The majority of these receptors attach within a canyon or pit that is somewhat protected from the environment allowing for a more extensive conservation of residues (*33*). LDL receptors attach to the highly exposed starlike mesa at the 5-fold axis of icosahedral symmetry of minor group HRVs. Surface residues can thus considerably vary for escape from the immunological defense while still maintaining low specificity but high affinity multimodular receptor binding. A similar approach is followed in nanotechnology to increase low affinity interactions employing highly repetitive structures.

In summary, using FCS, we have shown that several modules of the very-low-density lipoprotein receptor can bind simultaneously to the minor group human rhinovirus HRV2 thus enormously increasing the functional affinity of this interaction. Most remarkably, the attachment parameters of V333 could be explained by two binding events occurring in parallel; one with high affinity involving 3 modules and the second one with lower affinity involving 2 modules attaching to the starlike mesa at the 5-fold axis of icosahedral symmetry. We demonstrate that measurements of the interaction between a virus and a soluble derivative of its receptor can be carried out with minute amounts of sample in a very short time. FCS yields information beyond that accessible with other methods that require tedious immobilization procedures of one of the components (for example surface plasmon resonance techniques) and rendering sites unavailable for interaction. We are convinced that FCS is the method of choice for the analysis of the binding parameters underlying the interactions between viruses and receptors, antibodies, or virus-binding antivirals. In particular, viruses with high pathogenic potential can be analyzed since the FCS setup allows for easy containment of the sample.

ACKNOWLEDGMENT

We thank Irene Goesler for the preparation of HRV2.

REFERENCES

1. Semler, B. L., and Wimmer, E. (2002) *Molecular Biology of Picornaviruses*, ASM Press, Washington, DC 20036−2904.
2. Ledford, R. M., Patel, N. R., Demenczuk, T. M., Watanyar, A., Herbertz, T., Collett, M. S., and Pevear, D. C. (2004) VP1 sequencing of all human rhinovirus serotypes: Insights into genus phylogeny and susceptibility to antiviral capsid-binding compounds, *J. Virol. 78*, 3663−3674.
3. Uncapher, C. R., Dewitt, C. M., and Colonno, R. J. (1991) The major and minor group receptor families contain all but one human rhinovirus serotype, *Virology 180*, 814−817.
4. Staunton, D. E., Merluzzi, V. J., Rothlein, R., Barton, R., Marlin, S. D., and Springer, T. A. (1989) A cell adhesion molecule, ICAM-1, is the major surface receptor for rhinoviruses, *Cell 56*, 849−853.
5. Vlasak, M., Roivainen, M., Reithmayer, M., Goesler, I., Laine, P., Snyers, L., Hovi, T., and Blaas, D. (2005) The minor receptor group of human rhinovirus (HRV) includes HRV23 and HRV25, but the presence of a lysine in the VP1 HI loop Is not sufficient for receptor binding, *J. Virol. 79*, 7389−7395.
6. Marlovits, T. C., Abrahamsberg, C., and Blaas, D. (1998) Very-low-density lipoprotein receptor fragment shed from HeLa cells inhibits human rhinovirus infection, *J. Virol. 72*, 10246−10250.
7. Staunton, D. E., Dustin, M. L., Erickson, H. P., and Springer, T. A. (1990) The arrangement of the immunoglobulin-like domains of Icam-1 and the binding sites for LFA-1 and rhinovirus, *Cell 61*, 243−254.
8. Xing, L., Casasnovas, J. M., and Cheng, R. H. (2003) Structural analysis of human rhinovirus complexed with icam-1 reveals the dynamics of receptor-mediated virus uncoating, *J. Virol. 77*, 6101−6107.
9. Olson, N. H., Kolatkar, P. R., Oliveira, M. A., Cheng, R. H., Greve, J. M., McClelland, A., Baker, T. S., and Rossmann, M. G. (1993) Structure of a human rhinovirus complexed with its receptor molecule, *Proc. Natl. Acad. Sci. U.S.A. 90*, 507−511.
10. Kolatkar, P. R., Bella, J., Olson, N. H., Bator, C. M., Baker, T. S., and Rossmann, M. G. (1999) Structural studies of two rhinovirus serotypes complexed with fragments of their cellular receptor, *EMBO J. 18*, 6249−6259.
11. Nykjaer, A., and Willnow, T. E. (2002) The low-density lipoprotein receptor gene family: a cellular Swiss army knife?, *Trends Cell Biol. 12*, 273−280.
12. Verdaguer, N., Fita, I., Reithmayer, M., Moser, R., and Blaas, D. (2004) X-ray structure of a minor group human rhinovirus bound to a fragment of its cellular receptor protein, *Nat. Struct. Mol. Biol. 11*, 429−434.
13. Moser, R., Snyers, L., Wruss, J., Angulo, J., Peters, H., Peters, T., and Blaas, D. (2005) Neutralization of a common cold virus by concatemers of the third ligand binding module of the VLDL-receptor strongly depends on the number of modules, *Virology 338*, 259−269.
14. Ronacher, B., Marlovits, T. C., Moser, R., and Blaas, D. (2000) Expression and folding of human very-low-density lipoprotein receptor fragments: neutralization capacity toward human rhinovirus HRV2, *Virology 278*, 541−550.
15. Konecsni, T., Kremser, L., Snyers, L., Rankl, C., Kilar, F., Kenndler, E., and Blaas, D. (2004) Twelve receptor molecules attach per viral particle of human rhinovirus serotype 2 via multiple modules, *FEBS Lett. 568*, 99−104.
16. Querol-Audí, J., Fita, I., Konecsni, T., Wruss, J., Blaas, D., and Verdaguer, N. (2007) X-ray structure of a pentameric concatemer of the V3 module of the very-low density lipoprotein receptor bound to human rhinovirus type 2: Geometry constraints for multimodule binding, in preparation.
17. Haustein, E., and Schwille, P. (2003) Ultrasensitive investigations of biological systems by fluorescence correlation spectroscopy, *Methods 29*, 153−166.
18. Mischak, H., Neubauer, C., Berger, B., Kuechler, E., and Blaas, D. (1988) Detection of the human rhinovirus minor group receptor on renaturing Western blots, *J. Gen. Virol. 69*, 2653−2656.
19. Okun, V. M., Ronacher, B., Blaas, D., and Kenndler, E. (1999) Analysis of common cold virus (human rhinovirus serotype 2) by capillary zone electrophoresis: The problem of peak identification, *Anal. Chem. 71*, 2028−2032.
20. Maier, C., Rünzler, D., Schindelar, J., Grabner, G., Waldhäusl, W., Köhler, G., and Luger, A. (2005) G-protein-coupled glucocorticoid receptors on the pituitary cell membrane, *J. Cell Sci. 118*, 3353−3361.
21. Fass, D., Blacklow, S., Kim, P. S., and Berger, J. M. (1997) Molecular basis of familial hypercholesterolaemia from structure of LDL receptor module, *Nature 388*, 691−693.
22. Beglova, N., North, C. L., and Blacklow, S. C. (2001) Backbone dynamics of a module pair from the ligand-binding domain of the LDL receptor, *Biochemistry 40*, 2808−2815.
23. Kremser, L., Konecsni, T., Blaas, D., and Kenndler, E. (2004) Fluorescence labeling of human rhinovirus capsid and analysis by capillary electrophoresis, *Anal. Chem. 76*, 4175−4181.
24. Hewat, E. A., and Blaas, D. (1996) Structure of a neutralizing antibody bound bivalently to human rhinovirus 2, *EMBO J. 15*, 1515−1523.
25. Verdaguer, N., Blaas, D., and Fita, I. (2000) Structure of human rhinovirus serotype 2 (HRV2), *J. Mol. Biol. 300*, 1179−1194.
26. Meseth, U., Wohland, T., Rigler, R., and Vogel, H. (1999) Resolution of fluorescence correlation measurements, *Biophys. J. 76*, 1619−1631.
27. Schubert, F., Zettl, H., Hafner, W., Krauss, G., and Krausch, G. (2003) Comparative thermodynamic analysis of DNA−protein interactions using surface plasmon resonance and fluorescence correlation spectroscopy, *Biochemistry 42*, 10288−10294.
28. Jencks, W. P. (1981) On the attribution and additivity of binding energies, *Proc. Natl. Acad. Sci. U.S.A. 78*, 4046−4050.
29. Fisher, C., Beglova, N., and Blacklow, S. C. (2006) Structure of an LDLR-RAP complex reveals a general mode for ligand recognition by lipoprotein receptors, *Mol. Cell 22*, 277−283.
30. Mendelsohn, C. L., Wimmer, E., and Racaniello, V. R. (1989) Cellular receptor for poliovirus: molecular cloning, nucleotide sequence, and expression of a new member of the immunoglobulin superfamily, *Cell 56*, 855−865.
31. Bergelson, J. M., Shepley, M. P., Chan, B. M. C., Hemler, M. E., and Finberg, R. W. (1992) Identification of the Integrin VLA-2 as a Receptor for Echovirus-1, *Science 255*, 1718−1720.
32. Bergelson, J. M., Cunningham, J. A., Droguett, G., Kurt-Jones, E. A., Krithivas, A., Hong, J. S., Horwitz, M. S., Crowell, R. L., and Finberg, R. W. (1997) Isolation of a common receptor for Coxsackie B viruses and adenoviruses 2 and 5, *Science 275*, 1320−1323.
33. Rossmann, M. G. (1989) The canyon hypothesis. Hiding the host cell receptor attachment site on a viral surface from immune surveillance, *J. Biol. Chem. 264*, 14587−14590.

BI700262W